Interpolatory model reduction for component mode synthesis analysis of structures involving substructures with frequency-dependent parameters

L Cortés, Jean-Mathieu Mencik, Stéphane Méo

Interpolatory model reduction for component mode synthesis analysis of structures involving substructures with frequency-dependent parameters

Conference Paper · September 2016

CITATIONS
0

READS
19

3 authors:

Lluís Cortés
Institut National des Sciences Appliquées C…
9 PUBLICATIONS **11** CITATIONS
SEE PROFILE

Jean-Mathieu Mencik
Institut National des Sciences Appliquées C…
78 PUBLICATIONS **446** CITATIONS
SEE PROFILE

Stéphane Méo
University of Tours
47 PUBLICATIONS **137** CITATIONS
SEE PROFILE

Interpolatory model reduction for component mode synthesis analysis of structures involving substructures with frequency-dependent parameters

L. Cortés [1], **J.-M. Mencik** [1], **S. Méo** [2]
[1] INSA Centre Val de Loire, Université François Rabelais de Tours, LMR EA 2640, Campus de Blois, 3 Rue de la Chocolaterie, CS 23410, 41034 Blois Cedex, France
[2] Polytech Tours, Université François Rabelais de Tours, LMR EA 2640, 7 Avenue Marcel Dassault, 37000 Tours, France
e-mail: **jean-mathieu.mencik@insa-cvl.fr**

Abstract
An interpolatory model order reduction (MOR) strategy is proposed to compute the harmonic forced response of structures built up of substructures with frequency-dependent parameters. In this framework, the Craig-Bampton (CB) method is used for modeling each substructure by means of static modes and a reduced number of fixed-interface modes which are interpolated between several master frequencies. Emphasis is on the analysis of several substructures which can vibrate at different scales and, as such, do not need to be modeled with the same sets of interpolation points, depending on whether their modal density is low or high. For this purpose, an error indicator is developed to determine, through greedy algorithm procedure, the optimal number of interpolation points needed for each substructure. Additional investigations concern the selection of the fixed-interface modes which need to be retained for each substructure. Numerical experiments are carried out to highlight the relevance of the proposed approach, in terms of computational saving and accuracy.

1 Introduction

The problem of predicting the dynamic response of structures which are composed of substructures with frequency-dependent parameters is addressed in the present work. Those substructures may refer, for instance, to structural components and viscoelastic junctions connected to each other, where it is understood that the material characteristics of the junctions vary over the frequency domain. Also, the substructures are likely to vibrate at different scales, i.e., their modal densities can be largely disparate. Assessing the frequency response of this kind of multi-physics and multi-scale vibrating systems is the motivation behind the present work. Emphasis is placed on the development of efficient finite element (FE) based MOR approaches which are accurate and low-time consuming.

Recent works have demonstrated the potentiality of interpolatory MOR methods for analyzing dynamic models with parameter-dependent matrices [1, 2]. These techniques consist in computing a finite set of reduced-order bases at some interpolation points — i.e., at some discrete values of the varying parameters — and interpolating reduced matrices — i.e., once projected in the subspaces spanned by the reduced bases — between the interpolation points. One of the key idea in these methods is the consideration of a Modal Assurance Criterion (MAC) -based congruence transformation to ensure the compatibility among the coordinates systems of the reduced bases, i.e., between the interpolation points [1, 2]. For frequency-dependent matrices, another approach has been proposed in [3] which interpolates reduced bases of vibration modes, rather than projected matrices, between master frequencies. In this framework, the Craig-Bampton (CB) method [4] is

used for modeling substructures by means of static modes and reduced sets of fixed-interface modes which are thus interpolated, e.g., using Lagrange polynomials. The static modes are being kept constant and are computed from the stiffness matrices of the substructures expressed at a certain frequency f, e.g., $f = 0$. The interesting feature of this approach is that it involves interpolating a matrix of fixed-interface modes only, instead of interpolating several matrices and vectors in different ways which may penalize the determination of the subspaces between the interpolation points.

This technique will be considered and improved in the present paper for modeling structures involving several substructures with frequency-dependent parameters. The originality of the present work lies in the consideration of several substructures which can vibrate at different scales, i.e., they do not need to be modeled with the same sets of interpolation points. Here, an error indicator is proposed to determine, through greedy algorithm procedure, the optimal number of interpolation points — i.e., the number of master frequencies — for each substructure. The development of this error indicator follows from the analysis of the force balance equation on each interface between two connected substructures. It can be shown that this procedure is much more relevant than the usual one when a residual force vector is analyzed at a few excitation points, regardless of the coupling conditions between the substructures. Additional investigations are also proposed to determine the number of fixed-interface modes for modeling each substructure.

The rest of the paper is organized as follows. In Section 2, the basics of the CB method, for modeling a set of coupled substructures by means of static modes and fixed-interface modes, are recalled. In Section 3, the interpolatory MOR strategy is presented. The matrices of fixed-interface modes of the substructures are assessed and post-treated according to the MAC criterion proposed in [1, 2]. Also, the error indicator used to select the number of interpolation points for each substructure is derived. In Section 4, numerical experiments are carried out concerning an assembly of plates with two different frequency-dependent substructures and a frequency-independent substructure. The efficiency of the proposed approach is highlighted in comparison with the conventional CB method. Additional discussions are brought about the selection of the number of fixed-interfaces modes per substructure.

2 Craig Bampton method

The Craig Bampton (CB) method is one of the most popular Component Mode Synthesis (CMS) techniques which combine substructuring and model order reduction to solve large-scale dynamic systems in an efficient way. The method has been initiated in [4] and is recalled hereafter of the sake of clarity.

Consider the FE model of a structure which is composed of several substructures, see Figure 1. Each substructure is assumed to be linear, elastic and dissipative. Also, for the sake of simplicity, assumption is made that the FE meshes of the substructures are compatible across their coupling interfaces.

Consider a given substructure s. In the frequency domain, its dynamic equilibrium equation is given by

$$\left(-\omega^2\mathbf{M}^s + \mathtt{i}\omega\mathbf{C}^s + \mathbf{K}^s\right)\mathbf{q}^s = \mathbf{F}^s, \tag{1}$$

where $\mathbf{M}^s$, $\mathbf{C}^s$ and $\mathbf{K}^s$ are the mass, damping and stiffness matrices of the substructure, respectively, which are supposed to be real symmetric; $\mathbf{q}^s$ and $\mathbf{F}^s$ are the vectors of nodal displacements and nodal forces, respectively; also, ω is the angular frequency. Eq. (1) can be partitioned into boundary (B) and internal (I) degrees of freedom (DOFs) — i.e., those which belong and do not belong to the coupling interface, respectively —, as follows:

$$\left(-\omega^2\begin{bmatrix}\mathbf{M}^s_{\mathtt{BB}} & \mathbf{M}^s_{\mathtt{BI}}\\ \mathbf{M}^s_{\mathtt{IB}} & \mathbf{M}^s_{\mathtt{II}}\end{bmatrix} + \mathtt{i}\omega\begin{bmatrix}\mathbf{C}^s_{\mathtt{BB}} & \mathbf{C}^s_{\mathtt{BI}}\\ \mathbf{C}^s_{\mathtt{IB}} & \mathbf{C}^s_{\mathtt{II}}\end{bmatrix} + \begin{bmatrix}\mathbf{K}^s_{\mathtt{BB}} & \mathbf{K}^s_{\mathtt{BI}}\\ \mathbf{K}^s_{\mathtt{IB}} & \mathbf{K}^s_{\mathtt{II}}\end{bmatrix}\right)\begin{bmatrix}\mathbf{q}^s_{\mathtt{B}}\\ \mathbf{q}^s_{\mathtt{I}}\end{bmatrix} = \begin{bmatrix}\mathbf{F}^s_{\mathtt{B}}\\ \mathbf{F}^s_{\mathtt{I}}\end{bmatrix}. \tag{2}$$

Denote as $n^s_{\mathtt{B}}$ and $n^s_{\mathtt{I}}$ the number of boundary and internal DOFs, respectively. Within the CB framework, the vector of nodal displacements $\mathbf{q}^s_{\mathtt{I}}$ is expressed in terms of static modes $\{\boldsymbol{\chi}^s_j\}_{j=1}^{n^s_{\mathtt{B}}}$ and a reduced set of

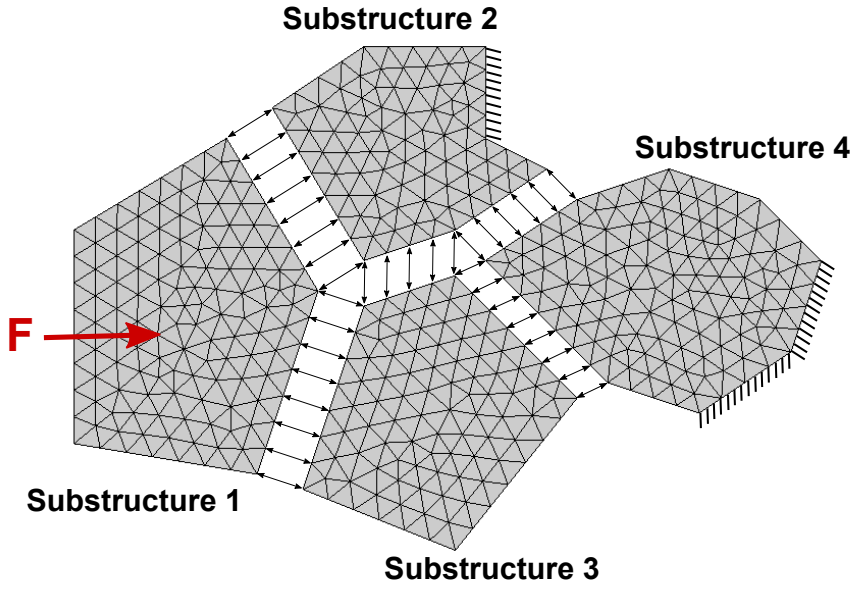

Figure 1: FE model of an abstract structure composed of four substructures.

fixed-interfaces modes $\{\tilde{\boldsymbol{\phi}}_j^s\}_{j=1}^{m_{\mathtt{I}}^s}$, where $m_{\mathtt{I}}^s \ll n_{\mathtt{I}}^s$, as follows:

$$\mathbf{q}_{\mathtt{I}}^s \approx \mathbf{X}^s \tilde{\mathbf{q}}_{\mathtt{B}}^s + \sum_{j=1}^{m_{\mathtt{I}}^s} \tilde{\boldsymbol{\phi}}_j^s \tilde{\alpha}_j^s \qquad \text{where} \qquad \tilde{\mathbf{q}}_{\mathtt{B}}^s \approx \mathbf{q}_{\mathtt{B}}^s, \tag{3}$$

where $\tilde{\mathbf{q}}_{\mathtt{B}}^s$ is the approximate vector of boundary DOFs — i.e., which results from the resolution of the CB model —, while $\tilde{\alpha}_j^s$ refers to generalized coordinates; also, $\mathbf{X}^s$ is the matrix of static modes, which is defined by:

$$\mathbf{X}^s = [\boldsymbol{\chi}_1^s \cdots \boldsymbol{\chi}_{n_{\mathtt{B}}^s}^s] = -(\mathbf{K}_{\mathtt{II}}^s)^{-1}\mathbf{K}_{\mathtt{IB}}^s. \tag{4}$$

On the other hand, the fixed-interface modes are the eigenvectors of the matrix pencil $(\mathbf{K}_{\mathtt{II}}^s, \mathbf{M}_{\mathtt{II}}^s)$. In matrix form, Eq. (3) is written by

$$\mathbf{q}_{\mathtt{I}}^s \approx \mathbf{X}^s \tilde{\mathbf{q}}_{\mathtt{B}}^s + \tilde{\boldsymbol{\Phi}}^s \tilde{\boldsymbol{\alpha}}^s, \tag{5}$$

where $\tilde{\boldsymbol{\Phi}}^s = [\tilde{\boldsymbol{\phi}}_1^s \cdots \tilde{\boldsymbol{\phi}}_{m_{\mathtt{I}}^s}^s]$ and $\tilde{\boldsymbol{\alpha}}^s = [\tilde{\alpha}_1^s \cdots \tilde{\alpha}_{m_{\mathtt{I}}^s}^s]^T$ are the $n_{\mathtt{I}}^s \times m_{\mathtt{I}}^s$ matrix of fixed-interface modes and the $m_{\mathtt{I}}^s \times 1$ vector of generalized coordinates, respectively. As a result, the vector of nodal displacements $\mathbf{q}^s$ is expressed by

$$\mathbf{q}^s \approx \begin{bmatrix} \tilde{\mathbf{q}}_{\mathtt{B}}^s \\ \tilde{\mathbf{q}}_{\mathtt{I}}^s \end{bmatrix} = \tilde{\mathbf{T}}^s \begin{bmatrix} \tilde{\mathbf{q}}_{\mathtt{B}}^s \\ \tilde{\boldsymbol{\alpha}}^s \end{bmatrix}, \tag{6}$$

where

$$\tilde{\mathbf{T}}^s = \begin{bmatrix} \mathbf{I} & \mathbf{0} \\ \mathbf{X}^s & \tilde{\boldsymbol{\Phi}}^s \end{bmatrix}. \tag{7}$$

As it turns out, the dynamic equilibrium equation (1) can be approximated through Galerkin procedure, as follows:

$$\left(-\omega^2 \tilde{\mathbf{M}}^s + \mathtt{i}\omega \tilde{\mathbf{C}}^s + \tilde{\mathbf{K}}^s\right) \begin{bmatrix} \tilde{\mathbf{q}}_{\mathtt{B}}^s \\ \tilde{\boldsymbol{\alpha}}^s \end{bmatrix} = \tilde{\mathbf{F}}^s, \tag{8}$$

where $\tilde{\mathbf{M}}^s$, $\tilde{\mathbf{C}}^s$ and $\tilde{\mathbf{K}}^s$ are reduced matrices of size $(n_{\mathtt{B}}^s + m_{\mathtt{I}}^s) \times (n_{\mathtt{B}}^s + m_{\mathtt{I}}^s)$. The matrices $\tilde{\mathbf{M}}^s$ and $\tilde{\mathbf{C}}^s$ are written as

$$\tilde{\mathbf{M}}^s = (\tilde{\mathbf{T}}^s)^T \mathbf{M}^s \tilde{\mathbf{T}}^s = \begin{bmatrix} \mathbf{M}_{\mathtt{BB}}^s + \mathbf{M}_{\mathtt{BI}}^s \mathbf{X}^s + (\mathbf{X}^s)^T \mathbf{M}_{\mathtt{IB}}^s + (\mathbf{X}^s)^T \mathbf{M}_{\mathtt{II}}^s \mathbf{X}^s & \mathbf{M}_{\mathtt{BI}}^s \tilde{\boldsymbol{\Phi}}^s + (\mathbf{X}^s)^T \mathbf{M}_{\mathtt{II}}^s \tilde{\boldsymbol{\Phi}}^s \\ (\tilde{\boldsymbol{\Phi}}^s)^T \mathbf{M}_{\mathtt{IB}}^s + (\tilde{\boldsymbol{\Phi}}^s)^T \mathbf{M}_{\mathtt{II}}^s \mathbf{X}^s & (\tilde{\boldsymbol{\Phi}}^s)^T \mathbf{M}_{\mathtt{II}}^s \tilde{\boldsymbol{\Phi}}^s \end{bmatrix}, \tag{9}$$

and

$$\tilde{\mathbf{C}}^s = (\tilde{\mathbf{T}}^s)^T \mathbf{C}^s \tilde{\mathbf{T}}^s = \begin{bmatrix} \mathbf{C}^s_{\mathtt{BB}} + \mathbf{C}^s_{\mathtt{BI}}\mathbf{X}^s + (\mathbf{X}^s)^T\mathbf{C}^s_{\mathtt{IB}} + (\mathbf{X}^s)^T\mathbf{C}^s_{\mathtt{II}}\mathbf{X}^s & \mathbf{C}^s_{\mathtt{BI}}\tilde{\mathbf{\Phi}}^s + (\mathbf{X}^s)^T\mathbf{C}^s_{\mathtt{II}}\tilde{\mathbf{\Phi}}^s \\ (\tilde{\mathbf{\Phi}}^s)^T\mathbf{C}^s_{\mathtt{IB}} + (\tilde{\mathbf{\Phi}}^s)^T\mathbf{C}^s_{\mathtt{II}}\mathbf{X}^s & (\tilde{\mathbf{\Phi}}^s)^T\mathbf{C}^s_{\mathtt{II}}\tilde{\mathbf{\Phi}}^s \end{bmatrix}. \tag{10}$$

Also, from Eq. (4), the matrix $\tilde{\mathbf{K}}^s$ is written as

$$\tilde{\mathbf{K}}^s = (\tilde{\mathbf{T}}^s)^T \mathbf{K}^s \tilde{\mathbf{T}}^s = \begin{bmatrix} \mathbf{K}^s_{\mathtt{BB}} + \mathbf{K}^s_{\mathtt{BI}}\mathbf{X}^s & \mathbf{0} \\ \mathbf{0} & (\tilde{\mathbf{\Phi}}^s)^T\mathbf{K}^s_{\mathtt{II}}\tilde{\mathbf{\Phi}}^s \end{bmatrix}. \tag{11}$$

Finally, in Eq. (8), $\tilde{\mathbf{F}}^s$ denotes the $(n^s_{\mathtt{B}} + m^s_{\mathtt{I}}) \times 1$ vector of excitations:

$$\tilde{\mathbf{F}}^s = (\tilde{\mathbf{T}}^s)^T \mathbf{F}^s = \begin{bmatrix} \mathbf{F}^s_{\mathtt{B}} + (\mathbf{X}^s)^T\mathbf{F}^s_{\mathtt{I}} \\ (\tilde{\mathbf{\Phi}}^s)^T\mathbf{F}^s_{\mathtt{I}} \end{bmatrix}. \tag{12}$$

The CB modeling of an assembly of N substructures, connected to each other through several coupling interfaces, can be readily addressed through classic FE assembly procedure. Define the global vector of generalized coordinates $\tilde{\boldsymbol{\alpha}}$:

$$\tilde{\boldsymbol{\alpha}} = \begin{bmatrix} \tilde{\boldsymbol{\alpha}}^1 \\ \vdots \\ \tilde{\boldsymbol{\alpha}}^N \end{bmatrix}. \tag{13}$$

Also, denote as $\tilde{\mathbf{q}}_{\mathtt{B}} \approx \mathbf{q}_{\mathtt{B}}$ the approximate global vector of boundary DOFs of the whole structure. The local and global vectors are linked as follows:

$$\begin{bmatrix} \tilde{\mathbf{q}}^s_{\mathtt{B}} \\ \tilde{\boldsymbol{\alpha}}^s \end{bmatrix} = \mathcal{L}^s \begin{bmatrix} \tilde{\mathbf{q}}_{\mathtt{B}} \\ \tilde{\boldsymbol{\alpha}} \end{bmatrix} \qquad s = 1, \ldots, N, \tag{14}$$

where $\mathcal{L}^s$ denotes a Boolean localization matrix for the substructure s. Hence, the Galerkin approximation of the dynamic equilibrium equation of the whole structure is expressed by

$$\left(-\omega^2\tilde{\mathbf{M}} + \mathtt{i}\omega\tilde{\mathbf{C}} + \tilde{\mathbf{K}}\right) \begin{bmatrix} \tilde{\mathbf{q}}_{\mathtt{B}} \\ \tilde{\boldsymbol{\alpha}} \end{bmatrix} = \tilde{\mathbf{F}}, \tag{15}$$

where

$$\tilde{\mathbf{M}} = \sum_{s=1}^{N} (\mathcal{L}^s)^T \tilde{\mathbf{M}}^s \mathcal{L}^s \quad , \quad \tilde{\mathbf{C}} = \sum_{s=1}^{N} (\mathcal{L}^s)^T \tilde{\mathbf{C}}^s \mathcal{L}^s \quad , \quad \tilde{\mathbf{K}} = \sum_{s=1}^{N} (\mathcal{L}^s)^T \tilde{\mathbf{K}}^s \mathcal{L}^s. \tag{16}$$

Also, $\tilde{\mathbf{F}}$ is the vector of external forces which are applied to the structure:

$$\tilde{\mathbf{F}} = \sum_{s=1}^{N} (\mathcal{L}^s)^T \tilde{\mathbf{F}}^s. \tag{17}$$

3 Interpolatory MOR

3.1 Introduction

In dynamic analysis, the mass, damping and stiffness matrices are often assumed to be frequency-independent and, consequently, a single CB reduced modeling is enough to analyze the dynamic response of a structure over a certain frequency range. Things are not so straightforward when materials having frequency-dependent parameters are dealt with. In this case, the mass, damping and stiffness matrices are no longer

constant, i.e., $\mathbf{M}^s = \mathbf{M}^s(\omega)$, $\mathbf{C}^s = \mathbf{C}^s(\omega)$ and/or $\mathbf{K}^s = \mathbf{K}^s(\omega)$ for some substructure s composing a whole structure. Also, the matrices of fixed-interface modes and static modes depend on the frequency — i.e., $\mathbf{\Phi}^s = \mathbf{\Phi}^s(\omega)$ and $\mathbf{X}^s = \mathbf{X}^s(\omega)$ —, meaning that they have to be recomputed at each discrete frequency considered in the frequency band of interest. This leads to computational costs which may largely exceed those involved when solving the standard unreduced FE problem — e.g., using a sparse solver —, which makes the CB method inefficient. To solve this issue, an interpolatory MOR strategy is proposed which aims at computing the matrices of fixed-interface modes and static modes of the substructures at a small number of master frequencies, only. The key idea is to linearly interpolate those matrices between the master frequencies so as to obtain approximate expressions — i.e., at any intermediary point between two consecutive master frequencies —, which can be done in a very fast way.

However, due to the frequency-dependency of the matrices, reduced bases of fixed-interface modes computed at different master frequencies span different subspaces with "coordinates systems" which are not necessarily compatible to each other. The issue may be viewed as to track each mode along the "master" frequency range, i.e., among all the reduced bases. As a result, directly interpolating the reduced bases of fixed-interface modes, without any mode tracking procedure, can be awkward. To solve this issue, a MAC-like procedure has been proposed in [1, 2]. In this framework, the reduced bases are first transformed into a set of generalized coordinates with respect to a reference subspace of the same order spanned by a reference basis. The proposed procedure enforces maximum correlation between the transformed bases and the reference basis. The choice of the reference basis is also addressed in [1] and it greatly determines the accuracy of the interpolation approximation. One possibility is to arbitrarily choose one of the master bases — i.e., those computed at the master frequencies — as being the reference subspace and transform the remaining master bases accordingly. However, there is no certainty that the chosen basis is the one that approximates the most important dynamics of the system best. A more convenient approach consists in computing the singular value decomposition (SVD) of the set of master bases in order to compute a meaningful reference basis, as proposed in [1]. Such an approach will be applied here to interpolate frequency-dependent reduced mode bases (see next subsection).

3.2 Mode basis interpolation

Consider a given substructure s and a set of M master angular frequencies $\{\Omega_p^s\}_{p=1}^M$ for which M matrices of fixed-interface modes $\{\tilde{\mathbf{\Phi}}_p^s\}_{p=1}^M$ — i.e., $\tilde{\mathbf{\Phi}}_p^s = \tilde{\mathbf{\Phi}}^s(\Omega_p)$ for $p \in \{1, \dots, M\}$ — are computed. Also, assume that the matrices $\tilde{\mathbf{\Phi}}_p^s$ have the same size $n_{\mathtt{I}}^s \times m_{\mathtt{I}}^s$.

Consider a so-called reference matrix of modes $\hat{\mathbf{\Psi}}^s$. As proposed in [1], the choice of a suitable reference basis is made by considering a singular value decomposition (SVD), as follows:

$$\begin{bmatrix} \tilde{\mathbf{\Phi}}_1^s & \cdots & \tilde{\mathbf{\Phi}}_M^s \end{bmatrix} = \mathbf{U}^s \mathbf{\Sigma}^s (\mathbf{V}^s)^T. \tag{18}$$

The reference matrix of modes $\hat{\mathbf{\Psi}}^s$ is then determined by considering the first $m_{\mathtt{I}}^s$ left singular vectors, i.e., those associated with the $m_{\mathtt{I}}^s$ highest singular values:

$$\hat{\mathbf{\Psi}}^s = \mathbf{U}^s(:, 1 : m_{\mathtt{I}}^s). \tag{19}$$

As explained in [1], each matrix of modes needs to be tightly connected with the reference matrix $\hat{\mathbf{\Psi}}^s$, which is done by considering the following modal coordinates transformation:

$$\hat{\mathbf{\Phi}}_p^s = \tilde{\mathbf{\Phi}}_p^s \hat{\mathcal{R}}_p^s \qquad p = 1, \dots, M, \tag{20}$$

where $\hat{\mathcal{R}}_p^s$ is a $m_{\mathtt{I}}^s \times m_{\mathtt{I}}^s$ orthogonal matrix — i.e., $(\hat{\mathcal{R}}_p^s)^T \hat{\mathcal{R}}_p^s = \hat{\mathcal{R}}_p^s (\hat{\mathcal{R}}_p^s)^T = \mathbf{I}$ — and $\hat{\mathbf{\Phi}}_p^s$ is the so-called transformed matrix of modes at master frequency Ω_p^s. Assume that the matrix $\hat{\mathbf{\Phi}}_p^s$ is strongly correlated, in

a MAC sense, to the reference matrix of modes $\hat{\boldsymbol{\Psi}}^s$. As it turns out, the matrix $\hat{\mathcal{R}}_p^s$ is found by solving a maximization problem:

$$\hat{\mathcal{R}}_p^s = \texttt{argmax}\,\texttt{tr}\left[(\hat{\boldsymbol{\Psi}}^s)^T\tilde{\boldsymbol{\Phi}}_p^s\hat{\mathcal{R}}_p^s\right] \qquad \text{subject to } (\hat{\mathcal{R}}_p^s)^T\hat{\mathcal{R}}_p^s = \hat{\mathcal{R}}_p^s(\hat{\mathcal{R}}_p^s)^T = \mathbf{I} \qquad p = 1,\ldots,M, \tag{21}$$

where $\texttt{tr}[\bullet]$ denotes the matrix trace. By considering an SVD of $(\tilde{\boldsymbol{\Phi}}_p^s)^T\hat{\boldsymbol{\Psi}}^s$ — i.e., $(\tilde{\boldsymbol{\Phi}}_p^s)^T\hat{\boldsymbol{\Psi}}^s = \hat{\mathbf{U}}_p^s\hat{\boldsymbol{\Sigma}}_p^s(\hat{\mathbf{V}}_p^s)^T$ —, the sought matrix $\hat{\mathcal{R}}_p^s$ is found to be [1, 2]:

$$\hat{\mathcal{R}}_p^s = \hat{\mathbf{U}}_p^s(\hat{\mathbf{V}}_p^s)^T \qquad p = 1,\ldots,M. \tag{22}$$

In the present work, a linear interpolation scheme of the matrix of modes is dealt with. Hence, for a substructure s having frequency-dependent parameters, a matrix $\hat{\mathbf{T}}_p^s$ (see Eq. (7)) can be defined at each master frequency Ω_p as

$$\hat{\mathbf{T}}_p^s = \begin{bmatrix}\mathbf{I} & \mathbf{0}\\ \mathbf{X}_p^s & \hat{\boldsymbol{\Phi}}_p^s\end{bmatrix}, \tag{23}$$

where $\mathbf{X}_p^s = \mathbf{X}^s(\Omega_p)$ is the matrix of static modes at Ω_p:

$$\mathbf{X}_p^s = -\mathbf{K}_{\texttt{II}}^s(\Omega_p)^{-1}\mathbf{K}_{\texttt{IB}}^s(\Omega_p). \tag{24}$$

If one assumes that the master frequencies $\{\Omega_p^s\}_{p=1}^M$ are sorted in ascending order, the interpolated transformed matrix of modes, at a given frequency ω between two consecutive master frequencies Ω_p^s and Ω_{p+1}^s, is given by

$$\hat{\mathbf{T}}^s(\omega) = \frac{\Omega_{p+1}^s - \omega}{\Omega_{p+1}^s - \Omega_p^s}\hat{\mathbf{T}}_p^s + \frac{\omega - \Omega_p^s}{\Omega_{p+1}^s - \Omega_p^s}\hat{\mathbf{T}}_{p+1}^s \qquad \text{for} \quad \Omega_p^s \le \omega < \Omega_{p+1}^s \qquad p = 1,\ldots,M-1. \tag{25}$$

As it turns out, the following alternative mode expansion can be proposed to assess the vector of nodal displacements of the substructure:

$$\mathbf{q}^s(\omega) \approx \begin{bmatrix}\hat{\mathbf{q}}_{\texttt{B}}^s\\ \hat{\mathbf{q}}_{\texttt{I}}^s\end{bmatrix} = \hat{\mathbf{T}}^s(\omega)\begin{bmatrix}\hat{\mathbf{q}}_{\texttt{B}}^s\\ \hat{\boldsymbol{\alpha}}^s\end{bmatrix} \qquad \text{for} \quad \Omega_p^s \le \omega < \Omega_{p+1}^s \qquad p = 1,\ldots,M-1, \tag{26}$$

where $\hat{\mathbf{q}}_{\texttt{B}}^s \approx \mathbf{q}_{\texttt{B}}^s$, while $\hat{\boldsymbol{\alpha}}^s = \hat{\boldsymbol{\alpha}}^s(\omega)$ is the $m_{\texttt{I}}^s \times 1$ vector of generalized coordinates associated to the interpolated reduced matrix of modes $\hat{\boldsymbol{\Phi}}^s(\omega)$. As a result, a modified Galerkin approximation of the dynamic equilibrium equation of the whole structure is to be considered, as follows:

$$\left(-\omega^2\hat{\mathbf{M}}(\omega) + \mathtt{i}\omega\hat{\mathbf{C}}(\omega) + \hat{\mathbf{K}}(\omega)\right)\begin{bmatrix}\hat{\mathbf{q}}_{\texttt{B}}\\ \hat{\boldsymbol{\alpha}}\end{bmatrix} = \hat{\mathbf{F}}, \tag{27}$$

where matrices $\hat{\mathbf{M}}(\omega)$, $\hat{\mathbf{K}}(\omega)$ and $\hat{\mathbf{C}}(\omega)$ are given by:

$$\hat{\mathbf{M}}^s(\omega) = \hat{\mathbf{T}}^s(\omega)^T\mathbf{M}^s(\omega)\hat{\mathbf{T}}^s(\omega), \tag{28}$$

$$\hat{\mathbf{C}}^s(\omega) = \hat{\mathbf{T}}^s(\omega)^T\mathbf{C}^s(\omega)\hat{\mathbf{T}}^s(\omega), \tag{29}$$

$$\hat{\mathbf{K}}^s(\omega) = \hat{\mathbf{T}}^s(\omega)^T\mathbf{K}^s(\omega)\hat{\mathbf{T}}^s(\omega). \tag{30}$$

3.3 Selection of master frequencies

The efficiency of the interpolatory MOR strategy is mainly determined by the number of master frequencies considered, since the computation of the matrices of modes at many master frequencies is likely to be cumbersome. On the other hand, the accuracy of the approximate solutions is proportional to the number of master frequencies. In other words, the smaller the number of master frequencies, the larger the frequency

gap between two master bases and, consequently, the greater the approximation error in interpolating those master bases. Thus, there is a tradeoff between computational cost and accuracy with respect to the number of master frequencies considered.

The analysis of a structure through "substructured" interpolatory MOR provides further benefits. In this framework, the interpolatory reduction is performed at the substructure level, i.e., the number of master frequencies may vary from one substructure to another. This offers the possibility to adapt the computational burden among the substructures. For instance, a stiff (frequency-dependent) substructure may be reduced using a very small number of master frequencies, whereas a more flexible (frequency-dependent) substructure would require a larger number of master frequencies for obtaining the same interpolation accuracy in a given frequency range. Therefore, frequency-dependent components with different numbers of master frequencies may coexist in a same CB model, together with frequency-independent components.

Such a strategy is proposed here. Notice that the number of master frequencies is defined at the substructure level and it determines the accuracy of the approximate solution. Then, the selection of the number of master frequencies per substructure appears to be a crucial task, which requires the use of an efficient error indicator (see next subsections).

A greedy-based selection algorithm which determines the required number of master frequencies per substructure is proposed. The procedure starts by defining, for each substructure s, a coarse set of equally-spaced master frequencies $\{\Omega_p^s\}_{p=1}^{M^s}$. The following steps are then considered:

1. Compute the matrix of transformed modes $\hat{\mathbf{\Phi}}_p^s$ at each master frequency Ω_p^s, see Eq. (20).
2. For each intermediary frequency ω considered within the frequency band $[\Omega_p^s\,,\,\Omega_{p+1}^s)$, compute the approximate solution, see Eq. (27).
3. Set as a new master frequency any intermediary frequency ω for which the error indicator $\bar{\epsilon}^s(\omega)$ exceeds the expected tolerance threshold, see Eq. (36).

The greedy algorithm runs until the error indicator $\bar{\epsilon}^s(\omega)$, for each substructure s, is under the expected tolerance threshold at each intermediary frequency ω. Notice that the matrices of fixed-interface modes $\{\tilde{\mathbf{\Phi}}_p^s\}_p$ and static modes $\{\mathbf{X}_p^s\}_p$ computed (and stored) at previous iterations do not need to be recomputed at subsequent iterations.

The success of the greedy algorithm greatly relies on the interpolatory error estimate. Computing the true error of the approximate solution is unfeasible since the exact solution would be required for that purpose. Instead, a computationally cheap error indicator must be considered (see next subsection). The error indicator must be tight enough so that the greedy algorithm does not overestimate the number of necessary master frequencies.

3.4 Error indicator

Assessing the efficiency of a MOR approach in structural dynamics usually involves ensuring that the vectors of input forces are well described by the approximate displacement solutions [5]. The issue hence consists in analyzing a set of residual force vectors at a few excitation points. One major drawback of this approach is that it is rather local and discards the analysis of the coupling conditions between the substructures, which is a crucial point when coupled systems are dealt with.

An alternative error analysis is proposed here to solve this issue. In this framework, the force balance equation on each interface between two (or more) connected substructures is invoked, which appears to be much more precise than the usual local error analysis based on residual forces. The proposed strategy is derived as follows.

Eq. (1) can be rewritten as

$$\mathbf{D}^s \begin{bmatrix} \mathbf{q}_{\mathtt{B}}^s \\ \mathbf{q}_{\mathtt{I}}^s \end{bmatrix} = \begin{bmatrix} \mathbf{F}_{\mathtt{B}}^s \\ \mathbf{F}_{\mathtt{I}}^s \end{bmatrix}, \tag{31}$$

where $\mathbf{D}^s = -\omega^2 \mathbf{M}^s(\omega) + \mathtt{i}\omega \mathbf{C}^s(\omega) + \mathbf{K}^s(\omega)$ is the dynamic stiffness matrix of a substructure s which, in matrix form, is expressed by

$$\mathbf{D}^s = \begin{bmatrix} \mathbf{D}_{\mathtt{BB}}^s & \mathbf{D}_{\mathtt{BI}}^s \\ \mathbf{D}_{\mathtt{IB}}^s & \mathbf{D}_{\mathtt{II}}^s \end{bmatrix}. \tag{32}$$

In Eq. (31), $\mathbf{F}_{\mathtt{B}}^s$ is the vector of boundary forces, which is given by $\mathbf{F}_{\mathtt{B}}^s = \mathbf{D}_{\mathtt{BB}}^s \mathbf{q}_{\mathtt{B}}^s + \mathbf{D}_{\mathtt{BI}}^s \mathbf{q}_{\mathtt{I}}^s$. On the other hand, by considering the approximate vectors of nodal displacements $\hat{\mathbf{q}}_{\mathtt{B}}^s$ and $\hat{\mathbf{q}}_{\mathtt{I}}^s$ (see Eq. (26)), the vector of boundary forces is rather expressed as $\mathbf{D}_{\mathtt{BB}}^s \hat{\mathbf{q}}_{\mathtt{B}}^s + \mathbf{D}_{\mathtt{BI}}^s \hat{\mathbf{q}}_{\mathtt{I}}^s$. As it turns out, the error made at the level of the substructure s is expressed by:

$$\hat{\mathbf{R}}_{\mathtt{B}}^s = \mathbf{F}_{\mathtt{B}}^s - (\mathbf{D}_{\mathtt{BB}}^s \hat{\mathbf{q}}_{\mathtt{B}}^s + \mathbf{D}_{\mathtt{BI}}^s \hat{\mathbf{q}}_{\mathtt{I}}^s). \tag{33}$$

Also, the error made at the level of a whole structure, made up of N substructures, is expressed by

$$\hat{\mathbf{R}}_{\mathtt{B}} = \sum_{s=1}^{N} (\mathcal{L}_{\mathtt{B}}^s)^T \hat{\mathbf{R}}_{\mathtt{B}}^s = \mathbf{F}_{\mathtt{B}} - \sum_{s=1}^{N} (\mathcal{L}_{\mathtt{B}}^s)^T (\mathbf{D}_{\mathtt{BB}}^s \hat{\mathbf{q}}_{\mathtt{B}}^s + \mathbf{D}_{\mathtt{BI}}^s \hat{\mathbf{q}}_{\mathtt{I}}^s), \tag{34}$$

where $\mathcal{L}_{\mathtt{B}}^s$ is a Boolean localization matrix concerning the boundary DOFs of a substructure s, and $\mathbf{F}_{\mathtt{B}} = \sum_{s=1}^{N} (\mathcal{L}_{\mathtt{B}}^s)^T \mathbf{F}_{\mathtt{B}}^s$ is the vector of boundary forces — i.e., the vector of input forces which are applied to the coupling interfaces between the substructures —, which is supposed to be known.

Notice that $\mathcal{L}_{\mathtt{B}}^s (\mathcal{L}_{\mathtt{B}}^{s'})^T \neq \mathbf{0}$ for two substructures s and s' coupled through a common interface. In this sense, a relative error made when expressing the force balance equation on the coupling interface between a substructure s and one (or more) connected substructure can be derived, as follows:

$$\epsilon^s(\omega) = \frac{\| \mathcal{L}_{\mathtt{B}}^s \hat{\mathbf{R}}_{\mathtt{B}} \|_2}{\| \mathbf{F} \|_2}. \tag{35}$$

where $\| \bullet \|_2$ denotes the $2-$norm, while $\mathbf{F}$ is the vector of input forces applied to the structure, which is known.

3.5 Scaled error indicator

The error indicator ϵ^s is expressed in terms of boundary forces, and, as such, does not reflect the true displacement error. To solve this issue, a scaled error indicator may be proposed as follows:

$$\bar{\epsilon}^s(\omega) = \frac{\tilde{\epsilon}_{\mathtt{q}}^{\mathtt{HR}}}{\epsilon^R} \epsilon^s(\omega), \tag{36}$$

where $\tilde{\epsilon}_{\mathtt{q}}^{\mathtt{HR}}$ is an estimate of the displacement error issued from the CB modeling:

$$\tilde{\epsilon}_{\mathtt{q}}^{\mathtt{HR}} = \frac{\| \tilde{\mathbf{q}} - \tilde{\mathbf{q}}^{\mathtt{HR}} \|_2}{\| \tilde{\mathbf{q}}^{\mathtt{HR}} \|_2}, \tag{37}$$

where $\tilde{\mathbf{q}}^{\mathtt{HR}}$ is the displacement vector issued from a "high resolution" CB modeling, i.e., with a large number of fixed-interface modes for each substructure (e.g., twice as many as those usually required). Also, ϵ^R is the error indicator for a given reference substructure R ($R \in \{1, \ldots, N\}$) which may be arbitrarily defined.

For practical purpose, both error terms $\tilde{\epsilon}_{\mathtt{q}}^{\mathtt{HR}}$ and ϵ^R can be set as constant, i.e., they need to be computed at one single master frequency only, e.g., the maximum frequency within the frequency band of interest. By considering the scaled error indicator $\bar{\epsilon}^s$, the difference between the boundary force error and the true displacement error is greatly reduced. In this way, a meaningful error tolerance threshold — e.g., 10% as this is usually done when estimating displacement errors — may be proposed, which can be directly compared to the scaled error indicator $\bar{\epsilon}^s$ at a low computational cost.

4 Numerical results

The interpolatory MOR strategy is used to analyze the frequency forced response of an assembly of three plates — say, substructures 1, 2 and 3 —, as shown in Figure 2. Substructures 1 and 3 are made of steel material and have similar dimensions 1.6 m $\times$ 4 m $\times$ 0.01 m; on the other hand, substructure 2 consists of an aluminum plate with dimensions 2 m $\times$ 4 m $\times$ 0.01 m. The FE meshes of the substructures are composed of 4-node isotropic thin plate elements with 3 DOFs per node, and are compatible across the coupling interfaces. Here, 90, 200 and 90 plate elements are respectively used to model substructures 1, 2 and 3, which yields 1287 DOFs for the whole structure. The structure has simply supported boundary conditions on one edge of each substructure, as shown in Figure 2. A 10N vertical harmonic point force is applied at location $(x, y, z) = (0.71 \text{ m}, 1 \text{ m}, 0 \text{ m})$ in substructure 1, while the harmonic response of the structure is assessed at a measurement point at the interface between substructures 1 and 2 (Figure 2).

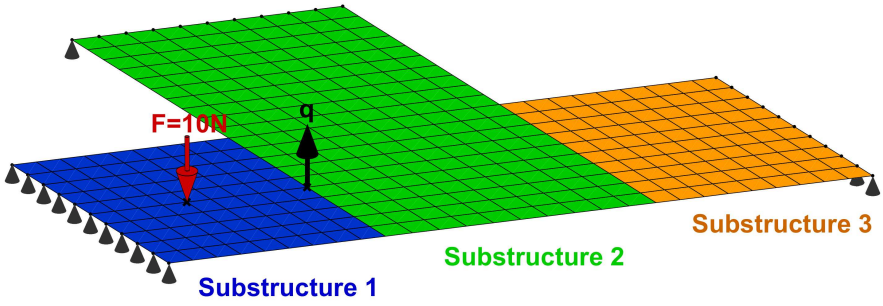

Figure 2: FE mesh of a three coupled plates structure with a 10N vertical point force in substructure 1 and a response measurement point at the interface between substructures 1 and 2.

The material properties of substructures 1, 2 and 3 are listed in Table 1. Here, the Young's moduli of substructures 1 and 3 are assumed to be frequency-dependent, i.e.:

$$E^s(\omega, \mathbf{x}) = E_0^s + \omega E_1^s(\mathbf{x}), \tag{38}$$

where $E_1^s(\mathbf{x})$ is the linear variation rate, which is here assumed to vary randomly in space (with mean value $\bar{E}_1^s$), and also, to be different between substructures 1 and 3. Also, the damping matrix of each substructure is assumed to be proportional to its stiffness matrix, as displayed in Table 1.

	Mass density	Elastic modulus E_0^s	Elastic modulus $\bar{E}_1^s$	Poisson's ratio	Damping proportionality
S1 (steel)	7800 kg/m^3	210 GPa	2.1 GPa.s/rad	0.31	4×10^{-5}
S2 (aluminum)	2700 kg/m^3	70 GPa	–	0.34	2×10^{-5}
S3 (steel)	7800 kg/m^3	210 GPa	0.21 GPa.s/rad	0.31	4×10^{-5}

Table 1: Material properties of substructures 1 (S1), 2 (S2) and 3 (S3).

The frequency response function (FRF) of the structure is assessed on a frequency band of $[0 \text{ Hz}, 50 \text{ Hz}]$ by considering 251 equally-spaced sample frequencies. For each sample frequency, the harmonic response is computed through CB modeling. The selection of the number of fixed-interface modes for each substructure is addressed in the following subsection.

4.1 Selection of fixed-interface modes

The accuracy of the CB solution is linked to the number of fixed-interface modes which are retained for modeling each substructure. As a rule of thumb, the selected modes are those for which the related eigenfrequencies are below a certain cut-off frequency, say twice the maximum frequency in the frequency band of

interest, i.e., $2f_{\max} = 2 \times 50 = 100$ Hz in the present case. Notice that for substructures having frequency-dependent parameters, the eigenfrequencies are frequency-dependent as well. Hence, the aforementioned selection criterion is to be applied by considering the eigenfrequencies computed at a certain frequency only, e.g., $f = f_{\max} = 50$ Hz. This yields 3, 25 and 7 fixed-interface modes for substructures 1, 2 and 3, respectively, that is, those for which the eigenfrequencies computed at $f_{\max}$ are below $2f_{\max}$.

As a first test, the FRF issued from the CB method (without interpolation) is compared to that issued from the FE method as shown in Figure 3. Also, the relative errors induced when computing the displacement and force vectors are displayed. Those displacement and force errors are defined as follows:

$$\tilde{\epsilon}_{\mathbf{q}}(\omega) = \frac{\|\tilde{\mathbf{q}} - \mathbf{q}\|_2}{\|\mathbf{q}\|_2} \quad , \quad \tilde{\epsilon}_{\mathbf{F}}(\omega) = \frac{\|\mathbf{D}\tilde{\mathbf{q}} - \mathbf{F}\|_2}{\|\mathbf{F}\|_2}, \tag{39}$$

where $\mathbf{D}$ is the dynamic stiffness matrix of the whole structure. Also, the errors $\tilde{\epsilon}_{\mathbf{q}}$ and $\tilde{\epsilon}_{\mathbf{F}}$ are compared to the error indicator ϵ^s (see Eq. (35)) for $s = 1, 3$, i.e., for the frequency-dependent substructures.

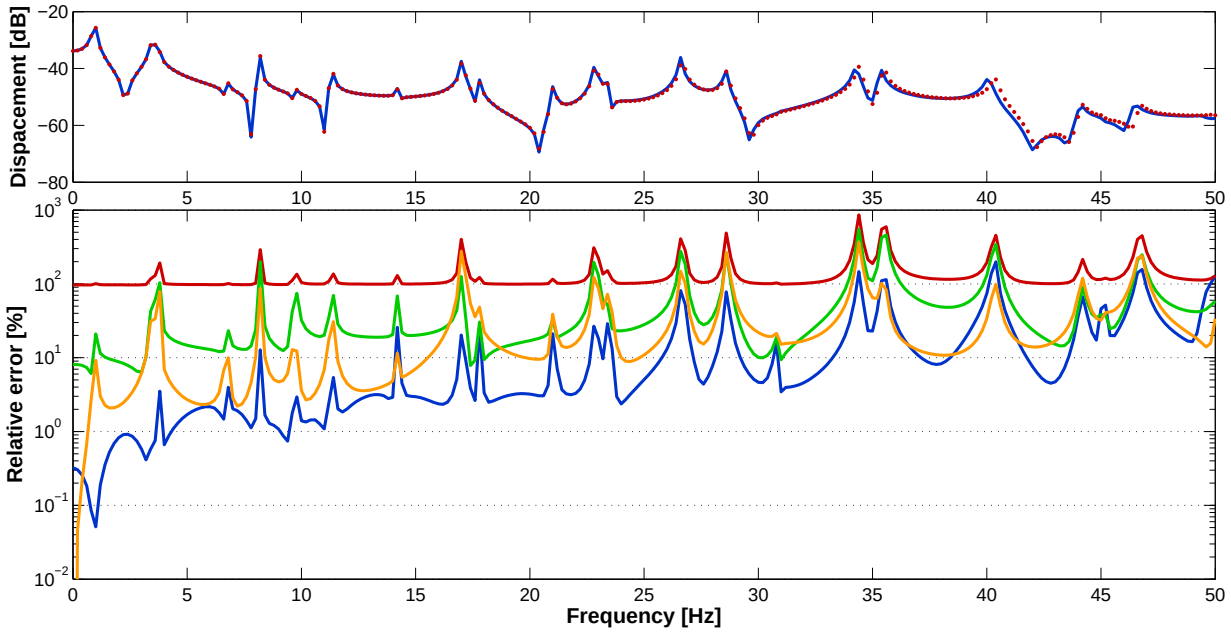

Figure 3: (top) FRF of the structure: — FE solution; · · · CB solution. (bottom) relative errors: — $\tilde{\epsilon}_{\mathbf{q}}(\omega)$; — $\tilde{\epsilon}_{\mathbf{F}}(\omega)$; — $\epsilon^1(\omega)$; — $\epsilon^3(\omega)$.

As it can be seen in Figure 3, the CB-based FRF appears to be close to the FE solution. Significant differences occur at high frequencies, which are due to the mode truncation process of the CB modeling. Regarding the errors, the true displacement error $\tilde{\epsilon}_{\mathbf{q}}$ is shown to be mostly greater than 10% over the frequency band. Notice that the force error $\tilde{\epsilon}_{\mathbf{F}}$ does not appear to be a good indicator of the true error $\tilde{\epsilon}_{\mathbf{q}}$ because it shows values exceeding 100% over the whole frequency band. On the contrary, the proposed error indicators ϵ^1 and ϵ^2 provide almost the same trends, in terms of curve shapes, than the displacement error.

As it turns out, the displacement error $\tilde{\epsilon}_{\mathbf{q}}$ is large especially at high frequencies. Hence, a higher cut-off frequency is required so as to include a larger number of fixed-interface modes for modeling each substructure. In Figure (4), the displacement error at $f_{\max}$ is plotted as a function of the cut-off frequency used to select the fixed-interface modes. As it can be seen, the cut-off frequency has to be much above $2f_{\max}$ so as to lower the errors at a satisfactory level. Thus, a cut-off frequency of $10f_{\max} = 500$ Hz is chosen which provides a displacement error under 1%. This corresponds to 23, 137 and 45 modes for substructures 1, 2 and 3, respectively.

It may be further observed in Figure 4 that the gap between the error indicators $\epsilon^1(\omega)$ and $\epsilon^3(\omega)$, and the true error $\tilde{\epsilon}_{\mathbf{q}}$, broadens as the cut-off frequency increases. This is even exacerbated for the force error $\tilde{\epsilon}_{\mathbf{F}}(\omega)$. This makes it necessary to use a scaled error indicator, see Eq. (36).

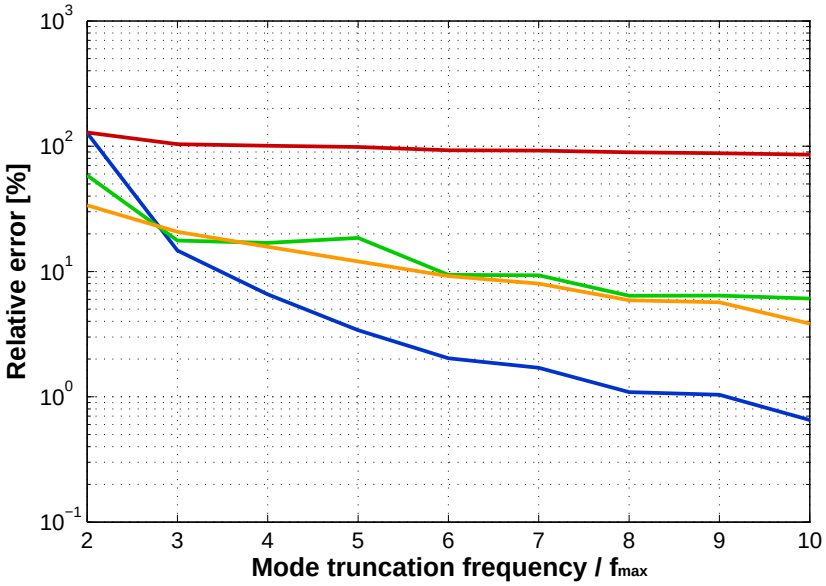

Figure 4: Errors at $f_{\max}$ as functions of the cut-off frequency. — $\tilde{\epsilon}_{\mathrm{q}}(\omega)$; — $\tilde{\epsilon}_{\mathrm{F}}(\omega)$; — $\epsilon^1(\omega)$; — $\epsilon^3(\omega)$.

4.2 Interpolatory MOR

The FRF of the structure is assessed using the interpolatory MOR strategy. Recall that a cut-off frequency of 500 Hz is considered to select the number of fixed-interface modes required for each substructure (see previous subsection). Substructure 2 is frequency-independent and, as such, does not requires interpolation of its modes. Regarding substructures 1 and 3, three equidistant master frequencies are initially considered, i.e., 0 Hz, 25 Hz and 50 Hz. Notice that the variation rate of the Young's modulus (Eq. (38)) of substructure 1 is ten times larger than that of substructure 3, so that different numbers of master frequencies may be required between these substructures. In fact, the greedy algorithm working with the scaled error indicator $\bar{\epsilon}^s$ and an error threshold of 10% (see Section 3.3) is used to determine the adequate number of master frequencies per substructure.

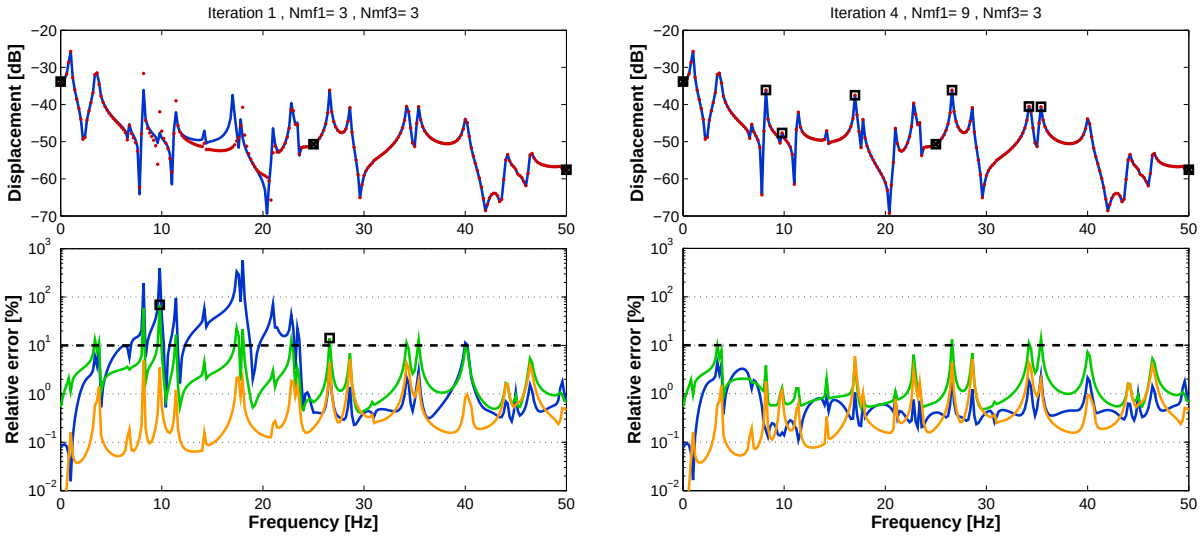

Figure 5: (top) FRF at the first (left) and last (right) iterations of the greedy algorithm: — FE solution; ··· interpolated solution; □ master frequencies for substructure 1; × master frequencies for substructure 3. (bottom) relative errors: — $\hat{\epsilon}_{\mathrm{q}}(\omega)$; — $\bar{\epsilon}^1(\omega)$; — $\bar{\epsilon}^3(\omega)$; - - - error threshold.

In Figure (5), the FRF is shown at the first and last iteration of the greedy algorithm, along with the true displacement error $\hat{\epsilon}_{\mathtt{q}}$:

$$\hat{\epsilon}_{\mathtt{q}}(\omega) = \frac{\|\hat{\mathbf{q}} - \mathbf{q}\|_2}{\|\mathbf{q}\|_2}. \tag{40}$$

Also, the scaled error indicators $\bar{\epsilon}^1(\omega)$ and $\bar{\epsilon}^3(\omega)$ are displayed.

At the first iteration where 3 master frequencies per substructure are considered, the computed FRF is clearly incorrect between the two first master frequencies. Both displacement error $\hat{\epsilon}_{\mathtt{q}}$ and scaled error indicator $\bar{\epsilon}^1$ are greater than the threshold, while $\bar{\epsilon}^3$ lays under the threshold. Consequently, two new master frequencies have been added for modeling substructure 1 (only) at the second iteration. The greedy algorithm ends once $\bar{\epsilon}^1$ and $\bar{\epsilon}^3$ are under the threshold at the intermediary points between the master frequencies. This occurs at the fourth iteration where 9 and 3 master frequencies are respectively considered for substructures 1 and 3. As expected, the true displacement error $\hat{\epsilon}_{\mathtt{q}}$ appears to be smaller than the threshold at the fourth iteration as shown in Figure 5.

Table 2 shows the execution times required at each iteration of the greedy algorithm to select the master frequencies and compute the FRF. Hence, the total execution time is 49.2 s. In comparison, it would have taken 724.6 s to compute the FRF with the CB method, i.e., by computing the fixed-interface modes and static modes of substructures 1 and 3 at every sampling frequency. This means more than 93% time saving in benefit of the proposed interpolatory MOR strategy.

	Computation of modes at new master frequencies	Interpolation of modes	Computation of FRF	Computation of scaled error indicators	Total time	Accumulated time
HR solution					2.6676 s	2.6676 s
Iteration 1	1.5750 s	0.2334 s	10.6168 s	0.2847 s	12.7436 s	15.4162 s
Iteration 2	0.2045 s	0.2404 s	10.4705 s	0.2851 s	11.2340 s	26.6515s
Iteration 3	0.2939 s	0.2557 s	10.4814 s	0.2765 s	11.3406 s	37.9933 s
Iteration 4	0.1046 s	0.2551 s	10.5619 s	0.2946 s	11.2505 s	49.2450 s

Table 2: Execution times involved in the interpolatory MOR strategy.

Also, the relevance of the proposed scaled error indicator $\bar{\epsilon}^s$ is analyzed when compared to the one based on residual forces. For this purpose, the following scaled force error indicator $\bar{\epsilon}_{\mathtt{F}}$ is considered:

$$\bar{\epsilon}_{\mathtt{F}}(\omega) = \frac{\tilde{\epsilon}_{\mathtt{q}}^{\mathtt{HR}}}{\epsilon^R} \frac{\|\mathbf{D}\hat{\mathbf{q}} - \mathbf{F}\|_2}{\|\mathbf{F}\|_2}, \tag{41}$$

The FRFs and errors at the first and last iteration of the greedy algorithm are shown in Figure 6. As it can be seen, the error indicator $\bar{\epsilon}_{\mathtt{F}}$ differs much more from the displacement error $\hat{\epsilon}_{\mathtt{q}}$ than the proposed error indicators $\bar{\epsilon}^1$ and $\bar{\epsilon}^3$, see Figure 5. In this case, the greedy algorithm stops at the second iteration where 4 master frequencies are considered for both substructures 1 and 3. Notice that the error indicator $\bar{\epsilon}_{\mathtt{F}}$ is global, i.e., the same number of master frequencies are added to each frequency-dependent substructure at each iteration of the greedy algorithm. In contrast, the proposed strategy enables the number of master frequencies to be optimized between the substructures. As a second drawback of the error indicator $\bar{\epsilon}_{\mathtt{F}}$, the displacement error cannot be lowered under the tolerance threshold at all sampling frequencies.

As it can be seen in Figure 6, the force error indicator $\bar{\epsilon}_{\mathtt{F}}$ exhibits a rather flat shape over the frequency band. This appears to be a consequence of the CB modeling in the sense that a modal reduction is performed at the DOF where the loading force is applied. The modal reduction ensures a good representation of the displacement field in substructures; however, the spatial distribution of the loading is not necessarily well captured by the same modal basis. Hence, significant errors may be introduced when approximating the loading term in the dynamic equilibrium equation. This may be observed in Figures 3 and 4, where the non-scaled force error $\tilde{\epsilon}_{\mathtt{F}}$ is around or even above 100% over the whole frequency band.

To clarify this point, consider the reciprocal problem in which the loading point and the measurement point are interchanged, as shown in Figure 7. In this case the point force is located on the coupling interface

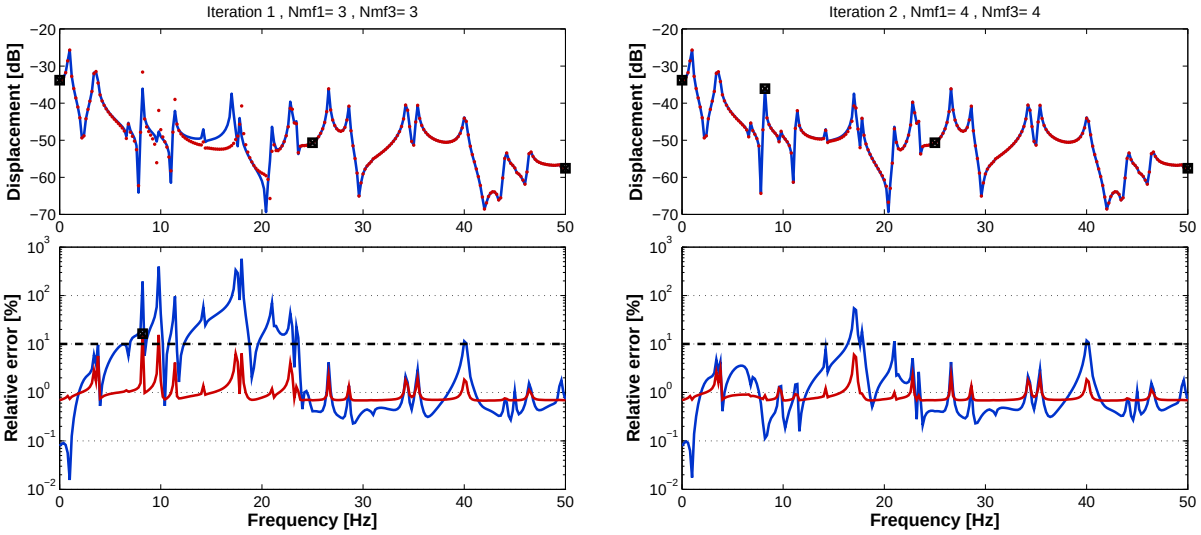

Figure 6: (top) FRF at first (left) and last (right) iterations of the greedy algorithm: — FE solution; ··· interpolated solution; □ master frequencies for substructure 1; × master frequencies for substructure 3. (bottom) relative errors: — $\hat{\epsilon}_{\mathrm{q}}(\omega)$; — $\bar{\epsilon}_{\mathrm{F}}(\omega)$; - - - error threshold.

between substructures 1 and 2, so that no mode truncation approximation is introduced when expressing the loading term. Figure 8 shows that the force error $\tilde{\epsilon}_{\mathrm{F}}$ decreases as the number of fixed-interface modes increases in a similar manner as the displacement error $\tilde{\epsilon}_{\mathrm{q}}$ and the error indicators ϵ^1 and ϵ^3. In this sense, the force error indicator $\bar{\epsilon}_{\mathrm{F}}$ (Eq. (41)) is likely to be much more accurate when compared to Figure 6.

Again, the FRFs and errors are computed as shown in Figure 9. By using either the force error indicator $\bar{\epsilon}_{\mathrm{F}}$, or the proposed indicators $\bar{\epsilon}^1$ and $\bar{\epsilon}^3$, the displacement error $\hat{\epsilon}_{\mathrm{q}}$ is reduced under the threshold of 10% after 5 iterations. However, the numbers of master frequencies are significantly different, i.e., 10 and 4 master frequencies for substructures 1 and 3 (respectively) with the proposed approach, against 11 master frequencies for both substructures 1 and 3 with the residual force approach. This clearly demonstrates the fact that the proposed MOR strategy works in a more efficient way to select the master frequencies.

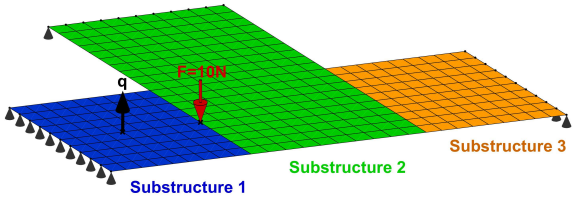

Figure 7: FE mesh of the three coupled plates structure with a 10N vertical point force acting on the interface between substructures 1 and 2, and a response measurement point in substructure 1.

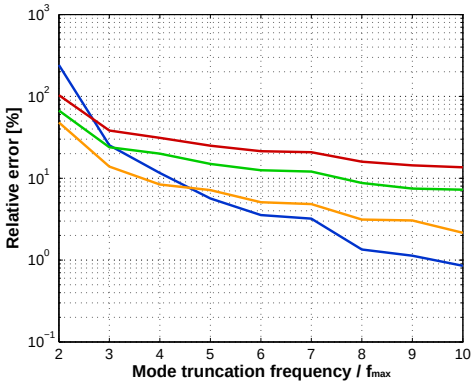

Figure 8: Errors at $f_{\max}$ (Figure 7) as functions of the cutoff frequency. — $\tilde{\epsilon}_{\mathrm{q}}(\omega)$; — $\tilde{\epsilon}_{\mathrm{F}}(\omega)$; — $\epsilon^1(\omega)$; — $\epsilon^3(\omega)$.

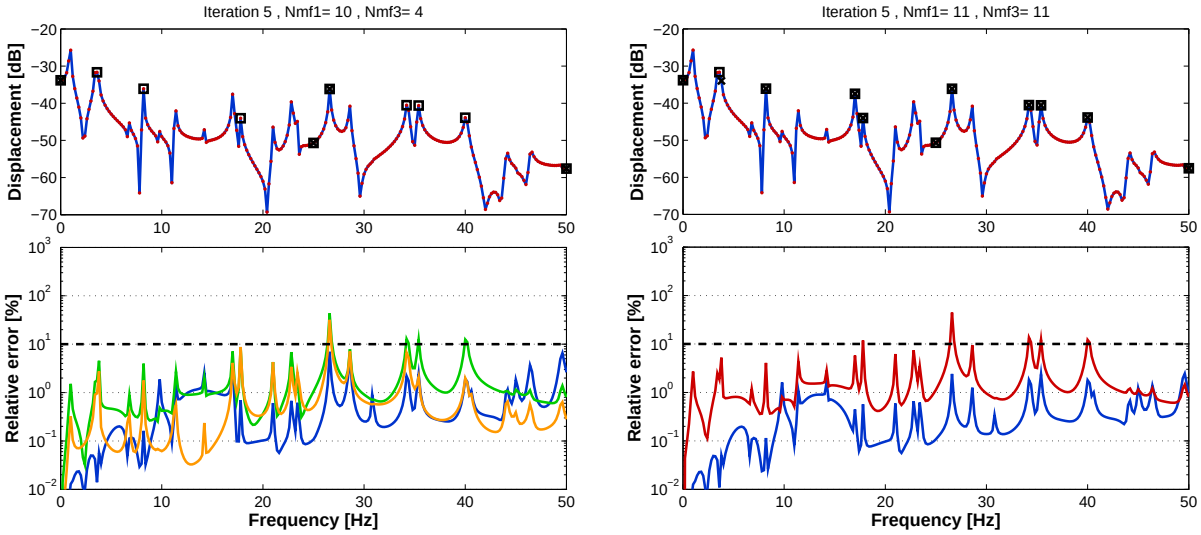

Figure 9: (top) FRF at the last iteration of the greedy algorithm, using the error indicator $\tilde{\epsilon}_{\mathrm{F}}$ (left) and the indicators ϵ^1 and ϵ^3 (right): — FE solution; · · · interpolated solution; □ master frequencies for substructure 1; × master frequencies for substructure 3. (bottom) relative errors: — $\hat{\epsilon}_{\mathrm{q}}(\omega)$; — $\bar{\epsilon}_{\mathrm{F}}(\omega)$; — $\bar{\epsilon}^1(\omega)$; — $\bar{\epsilon}^3(\omega)$; - - - error threshold.

4.3 Conclusions

An interpolatory MOR strategy has been proposed to compute the forced response of structures composed of substructures with frequency-dependent parameters. The CB method has been considered for modeling the substructures, and a linear interpolation scheme has been proposed to approximate the matrices of substructure modes between a set of master frequencies. The main advantage of the proposed MOR strategy lies in the consideration of an error indicator which enables the number of master frequencies to be modulated and optimized among the substructures. The selection of those master frequencies is automatically achieved through greedy algorithm. Several test cases have been carried out which clearly demonstrate the efficiency of the proposed approach.

Acknowledgements

The authors express their thanks for the financial support provided by “Le Commissariat à l’énergie atomique et aux énergies alternatives (CEA)” and “La Région Centre”.

References

[1] H. Panzer, J. Mohring, R. Eid, B. Lohmann, *Parametric Model Order Reduction by Matrix Interpolation*, Automatisierungstechnik, Vol. 58, No. 8 (2010), pp. 475–484.

[2] D. Amsallem, C. Farhat, *An Online Method for Interpolating Linear Parametric Reduced-Order Models*, SIAM Journal on Scientific Computing, Vol. 33, No. 5 (2011), pp. 2169–2198.

[3] R. Ohayon, C. Soize, *Clarification about Component Mode Synthesis Methods for Substructures with Physical Flexible Interfaces*, International Journal of Aeronautical and Space Sciences, Vol. 15 (2014), pp. 113–122.

[4] R. R. Craig, Jr., M. C. C. Bampton, *Coupling of substructures for dynamic analyses.*, AIAA Journal, Vol. 6, No. 7 (1968), pp. 1313–1319.

[5] U. Hetmaniuk, R. Tezaur, C. Farhat, *An adaptive scheme for a class of interpolatory model reduction methods for frequency response problems*, International Journal for Numerical Methods in Engineering, Vol. 93, No. 10 (2013), pp. 1109–1124.